JOURNAL OF COMPUTATIONAL PHYSICS 48, 344–365 (1982)

A Multigrid Method for the Transonic Full Potential Equation Discretized with Finite Elements on an Arbitrary Body Fitted Mesh

HERMAN DECONINCK AND CHARLES HIRSCH

Department of Fluid Mechanics, Vrije Universiteit Brussel, 1050 Brussels, Belgium

Received January 15, 1982

A multigrid method for the acceleration of transonic potential flow calculations based on a Galerkin finite element approach is described. In order to allow the use of arbitrary body fitted meshes, it is necessary to introduce nonuniform interpolation and residual weighting. Emphasis is put on the construction of these operators consistent with the finite element approximation, while standard successive line overrelaxation is used as a smoothing step. Substantial convergence acceleration is obtained and results are presented for different transonic flow configurations including shocks.

INTRODUCTION

The multigrid method was originally introduced for the solution of the system of equations obtained from the finite difference (FD) discretization of elliptic partial differential equations by Fedorenko [1]; it was extended by Bakhalov [2] and further developed by Brandt [16]. It is based on the idea that corrections for the solution on a fine grid can be effectively approximated on a coarse grid with the help of the common underlying differential equation.

Finite element (FE) applications were soon recognized and at the present time the mathematical foundations are even better established than in the FD case, although practical implementations are rare. Convergence proofs under fairly general conditions for elliptic boundary value problems were obtained by Nicolaides [3, 4], Hackbush [5], and others. Two of the basic conclusions of these investigations are that the convergence of the multigrid methods is independent of the step size and that the amount of computational work for solving the discrete system of n unknowns is proportional to n. Practical aspects of the FE implementation on model problems are given by Brandt [6] and by Nicolaides [7], who describes extensive numerical results obtained for a Poisson eqution and another elliptic equation with variable coefficients and mixed boundary conditions, both on a uniformly discretized rectangular domain. These results confirm the convergence rates obtained with finite differences.

In transonic flow computations, the first multigrid solutions have been proposed by South and Brandt [8], with the transonic small perturbation equation and successive

0021-9991/82/120344-22$02.00/0

Copyright © 1982 by Academic Press, Inc.
All rights of reproduction in any form reserved.

line relaxation (SLOR) as the smoothing operator. Problems were encountered in the treatment of the boundary conditions and in calculations on nonuniform and curvilinear grids, probably due either to a lack of smoothing on a fine grid before passing to a coarser one or to an unsatisfactory residual weighting. Jameson [9] solved the transonic full potential equation on an arbitrary mesh and obtained very satisfying results with a generalized ADI as the smoothing step. As in most other applications, these multigrid methods are implemented on a rectangular (or circular) uniform computational mesh obtained from a mapping of the original physical curvilinear mesh; this allows uniform interpolations. This approach is appropriate in cases where the physical problem and boundary conditions are transformed by a global coordinate transformation as in most finite difference methods. The classical FE approach, however, handles the problem in the physical plane and uses only a local mapping of each curvilinear element to a reference parent element to facilitate the volume integrations needed in the computation.

Simple uniform interpolation is only obtained if the fine mesh elements are uniform subdivisions of a coarse grid element. This would pose a severe limit on the finest mesh that can be achieved, since only the mesh points of the coarsest mesh could be chosen in an arbitrary way. Therefore nonuniform interpolation and residual weighting is introduced in this paper, preserving the same flexibility with respect to the geometry as the usual FE methods. An advantage of the FE treatment is that the method leads to natural choices for the interpolation and weighting, even on the boundaries of the domain.

Indeed, a simple but artificial residual injection following the lines of FD methods has been tried with poor results, confirming the observations of Nicolaides [7] on a simple rectangular domain. It turns out that the amount of additional work due to the nonuniformity is reduced because the same numerical coefficients are needed for coarse to fine interpolations as for the fine to coarse weighting.

In the present investigation, successive line relaxation with downstream sweep direction is used as the smoothing component. Alternatively, this smoothing operator can be replaced by the FE ADI method developed in the past [10].

Numerical experiments on channel, single airfoil, and cascade geometries indicate a substantial convergence acceleration compared to the grid refinement technique which consists in the application of SLOR to successively finer grids with the previous coarse grid solution as the initial approximation.

Equation and FE Approximation with Isoparametric Elements

A brief account of the FE treatment is given here. More details can be found in previous publications and the references contained therein [13–15].

The potential equation in conservative form is given by

$$\partial_x(\rho\phi_x) + \partial_y(\rho\phi_y) = 0, \tag{1}$$

where x and y are the Cartesian coordinates in the physical plane and ϕ_x, ϕ_y are the velocity components.

The density ρ is obtained from the isentropic relation

$$\rho = \rho_t [1 - ((\gamma - 1)/\gamma r T_t)(\phi_x^2 + \phi_y^2)]^{1/\gamma - 1}, \tag{2}$$

where ρ_t and T_t are stagnation density and temperature, and γ is the ratio of specific heats.

In transonic flow regime, equation (1) is mixed elliptic–hyperbolic and allows different weak solutions for a given set of boundary conditions. If proper viscosity terms are added to the equation, one is certain to obtain a unique solution which is equal to the physical solution except for a small region around shocks [11].

The artificial density form of the artificial viscosity terms (due to Hafez *et al.* [12]) is particularly well suited for FE applications and works satisfactorily for flows with Mach numbers up to 1.5 [14, 15]. It is obtained by giving an upwind bias to the density which is replaced by

$$\tilde{\rho} = \rho - \mu \rho \underset{s}{\leftarrow} \Delta s \tag{3a}$$

where $\rho \underset{s}{\leftarrow}$ is the upwind derivative of ρ along the streamwise direction s, Δs is the mesh spacing and μ is a switching function with cutoff Mach number M_c which controls the amount of artificial viscosity:

$$\mu = \max(0, 1 - M_c^2/M^2). \tag{3b}$$

A finite element weighted residual approach is based on the weak formulation of (1) given by

$$R(\phi) = \int_S \tilde{\rho} \nabla W \nabla \phi \, dS - \oint_s W \tilde{\rho} \frac{\partial \phi}{\partial n} ds = 0 \tag{4}$$

for any continuous test function W, where S is the physical flow domain with boundary s. The functional $R(\phi)$ is called the residual. The integral over the boundary is the expression of the Neumann boundary conditions (BC) which are part of the problem specification. Three types of geometry are considered, each giving different specific Neuman BC: channel geometry, single airfoil and cascade geometry. Channel walls and blade or profile boundaries require the no-flux condition

$$\tilde{\rho}(\partial \phi / \partial n) = 0.$$

Points belonging to periodic boundaries in cascade geometries are treated as interior points by letting corresponding periodic points coincide [14]. At inlet and outlet boundaries, either the solution is given (Dirichlet condition) or the mass flow rate $\tilde{\rho}(\partial \phi / \partial n)$ is specified directly or in an iterative way by applying a Kutta Youkowski condition at the trailing edge. The far field condition for the single airfoil geometry is also introduced by forcing the known mass flow rate through the far field boundary.

An FE approximation of a function $\phi(x, y)$ is obtained by defining a finite-dimensional space S^h with basis functions $N_{ij}^h(x, y)$ attached to a set of meshpoints (i, j) spread over the flow domain S:

$$\phi^h(x, y) = \sum_{i,j} \phi_{ij}^h N_{ij}^h(x, y), \tag{5}$$

where ϕ_{ij}^h are the meshpoint values of ϕ^h and h the typical mesh size characteristic of the space S^h. It follows from (5) that

$$\begin{aligned} N_{ij}^h(x_{kl}^h, y_{kl}^h) = \delta_{ij}^{kl} &= 1 \qquad \text{for} \quad (i, j) = (k, l), \\ &= 0 \qquad \text{otherwise.} \end{aligned} \tag{6}$$

A discrete Galerkin approximation for the weak form (4) is found by taking a finite number of test functions W, namely, the basis functions of space S^h, giving the following nonlinear system of equation for the meshpoint values

$$R_{ij}^h = \sum_{k,l} \phi_{kl}^h K_{ij}^{kl}(\phi^h) - f_{ij}^h = 0, \tag{7}$$

where $K(\phi^h)$ is the stiffness matrix and f^h the contribution of the Neuman BC

$$K_{ij}^{kl}(\phi^h) = \int_S \tilde{\rho}(\phi^h) \nabla N_{kl}^h \nabla N_{ij}^h \, dS \qquad \text{and} \qquad f_{ij}^h = \int_s \tilde{\rho} \frac{\partial \phi}{\partial n} N_{ij}^h \, ds. \tag{8}$$

It is well known that exactly the same expression for the residual is found by solving the discrete minimization problem in S^h in cases where a minimum principle equivalent to the equation can be formulated (as in the fully elliptic subsonic case).

Expression (7) for the residual is developed in the physical plane and written in physical coordinates. It can be evaluated for any trial function ϕ after a choice of the type of element has been made which determines the type of basis functions of the space S^h. In [15], bilinear and biquadratic Lagrange elements have been used, the latter allowing third-order accuracy and parabolic approximation of the boundaries. With these elements, the integrations over an element surface (Eq. (8)) are usually carried out with Gauss quadrature after transformation of the arbitrarily shaped element to a unit square. In the standard FE treatment, this transformation is the locally defined isoparametric mapping

$$x^h(\xi^h, \eta^h) = \sum_{i,j} x_{ij}^h N_{ij}^h(\xi^h, \eta^h), \tag{9a}$$

$$y^h(\xi^h, \eta^h) = \sum_{i,j} y_{ij}^h N_{ij}^h(\xi^h, \eta^h), \tag{9b}$$

which is completely determined by the mapping of the meshpoints of the space S^h causing arbitrarily located meshpoints of the grid $S^{h/2}$ not to be mapped uniformly in the (ξ^h, η^h) plane.

The discrete nonlinear system (Eq. (7)) has been solved with the usual iterative methods such as successive line overrelaxation (SLOR) and approximate factorization (ADI) for which an FE version was developed [10]. The simple SLOR method is reliable but extremely slow because it eliminates effectively only the errors with wavelength comparable to the meshwidth h. Substantial convergence acceleration was achieved by solving the series of $N+1$ problems

$$R_{ij}^{2^n h} = 0, \qquad n = N, N-1, \ldots, 1, 0, \tag{10}$$

defined in the space $S^{2^n h}$, where the errors of wavelength $2^n h$ are eliminated effectively and the computational effort is reduced.

In this grid refinement technique, the influence of the coarse meshes is only felt through the initial approximation for the next finer mesh, while in the full multigrid approach described subsequently, the coarse grid equations are modified in order to represent meaningful approximations of the fine grid corrections.

Multigrid Algorithm

The multigrid approach is based on a different treatment of low- and high-frequency errors in the approximate solution: the high-frequency error components can only be resolved on a fine grid and are fortunately eliminated efficiently by existing relaxation techniques. Low-frequency components on the other hand are nearly unaffected by relaxation, but they are scaled with the dimensions of the physical domain and hence can be eliminated on a coarser grid where the computational effort is lower and the propagation of corrections through the domain is much more rapid.

We consider the system of nonlinear equations (Eq. (7)) constructed on the finest mesh with characteristic spacing h

$$R^h(\phi^h) = K^h(\phi^h) - f^h = 0. \tag{11}$$

This may be written in correction form with respect to a known approximate solution ϕ_n^h as

$$\hat{K}^h(\delta\phi^h) = K^h(\phi_n^h + \delta\phi^h) - K^h(\phi_n^h) = -R^h(\phi_n^h), \tag{12}$$

where the unknowns are now the correction $\delta\phi^h$ given by

$$\phi^h = \phi_n^h + \delta\phi^h. \tag{13}$$

Supposing that the high-frequency errors have been eliminated effectively by means of a smoothing operation such as SLOR or ADI, the correction $\delta\phi^h$ and the residual $R^h(\phi^h)$ may be considered as smoothly varying quantities for which an approximation on a coarser grid makes sense. This mesh with typical spacing $2h$ is obtained by dropping the odd-numbered coordinate lines of the mesh S^h. An updated approx-

imation ϕ^h_{n+1} can be calculated according to Eq. (13) by interpolating the coarse grid approximation $\delta\phi^{2h}$ for $\delta\phi^h$ back to the original mesh:

$$\phi^h_{n+1} = \phi^h_n + I^h_{2h}\delta\phi^{2h}, \tag{14}$$

where I^h_{2h} is the coarse to fine grid function interpolation operator called *prolongation*. The coarse grid approximation $\delta\phi^{2h}$ for the fine grid correction is the solution to the following equation on the coarse mesh:

$$\hat{K}^{2h}(\delta\phi^{2h}) = -{}^R I^{2h}_h R^h(\phi^h_n). \tag{15}$$

The fine to coarse residual restriction operator ${}^R I^{2h}_h$ constructs a meaningful approximation to the coarse grid residual R^{2h} based on the smoothly varying fine grid residuals.

By defining a coarse grid solution ϕ^{2h} as the approximation of ϕ^h on the coarse grid

$$\phi^{2h} = I^{2h}_h \phi^h_n + \delta\phi^{2h}, \tag{16}$$

where I^{2h}_h is the function restriction, Eq. (15) takes again the usual form of Eq. (11);

$$K^{2h}(\phi^{2h}) = f^{2h}. \tag{17}$$

Here the right-hand side is a known function of the fine grid approximate solution

$$f^{2h} = -{}^R I^{2h}_h R^h(\phi^h_n) + K^{2h}(I^{2h}_h \phi^h_n), \tag{18}$$

and $\delta\phi^{2h}$ can be eliminated from updating formula (14) by means of (16):

$$\phi^h_{n+1} = \phi^h_n + I^h_{2h}(\phi^{2h} - I^{2h}_h \phi^h_n). \tag{19}$$

The solution ϕ^{2h} in turn can be approximated on the mesh S^{4h} when it is sufficiently smooth, i.e., the whole procedure can be applied in a recursive way to Eq. (17). This nonlinear algorithm (FAS scheme) is due to Brandt [16], who describes an adaptive strategy for the transition to a coarser or finer grid depending on the convergence level and speed on a particular grid. A simpler fixed strategy has been used in the present work [7]: Starting on the finest mesh with spacing h, one line overrelaxation sweep is performed followed by the transition to the next coarse grid by means of Eqs. (17) and (18) until the coarsest grid is reached. On the coarsest grid, some additional relaxation sweeps are performed and the solution of the next finer grid is updated by means of Eq. (19). This is followed by one relaxation step until the second finest grid is reached. The cycle terminates with the updating of the finest grid approximate solution with the help of Eq. (19).

As distinct from FD approaches, the interpolation operators I^{2h}_h, I^h_{2h}, and ${}^R I^{2h}_h$ are not arbitrary but based on the FE interpolation spaces S^h and S^{2h}. They are considered in more detail in the following sections.

THE COARSE TO FINE GRID FUNCTION INTERPOLATION: OPERATOR I_{2h}^h

The only natural choice for the interpolation of a coarse mesh function ϕ^{2h} to a fine mesh location (x_{ij}^h, y_{ij}^h) is to use the value of ϕ^{2h} in the location (x_{ij}^h, y_{ij}^h) given by the FE approximation in space S^{2h}:

$$[I_{2h}^h \phi^{2h}]_{ij} = \phi^{2h}(x_{ij}^h, y_{ij}^h) = \sum_{k,l} I_{kl}^{ij} \phi_{kl}^{2h}, \tag{20}$$

where the matrix I_{kl}^{ij} is given by

$$I_{kl}^{ij} = N_{kl}^{2h}(x_{ij}^h, y_{ij}^h). \tag{21}$$

On an arbitrary mesh, this results in nonuniform interpolation coefficients I_{kl}^{ij} and with bilinear elements, for instance (Fig. 1), uniform interpolation is only obtained if the fine grid meshpoints are situated in the middle of the coarse grid element sides and in the center, in this case only giving the simple formula (Fig. 1a)

$$\begin{aligned}
&[I_{2h}^h \phi^{2h}]_C = \tfrac{1}{4}(\phi_1^{2h} + \varphi_2^{2h} + \phi_3^{2h} + \phi_4^{2h}) && \text{for the centernode,} \\
&[I_{2h}^h \phi^{2h}]_M = \tfrac{1}{2}(\phi_i^{2h} + \phi_j^{2h}) && \text{for the midside node } i-j, \\
&[I_{2h}^h \phi^{2h}]_i = \phi_i^{2h} && \text{for the corner nodes (identity).}
\end{aligned} \tag{22}$$

It follows that simple uniform interpolation is only possible for uniform refinements of the coarsest mesh, which could itself be chosen arbitrarily.

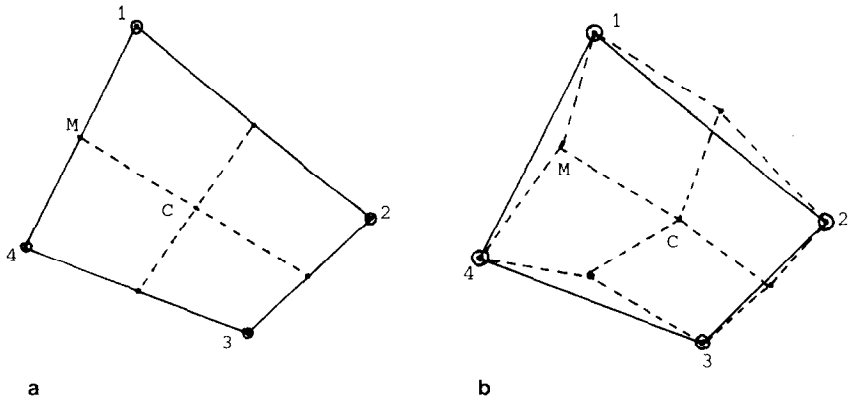

FIG. 1. (a) Uniform interpolation. (b) Nonuniform interpolation.

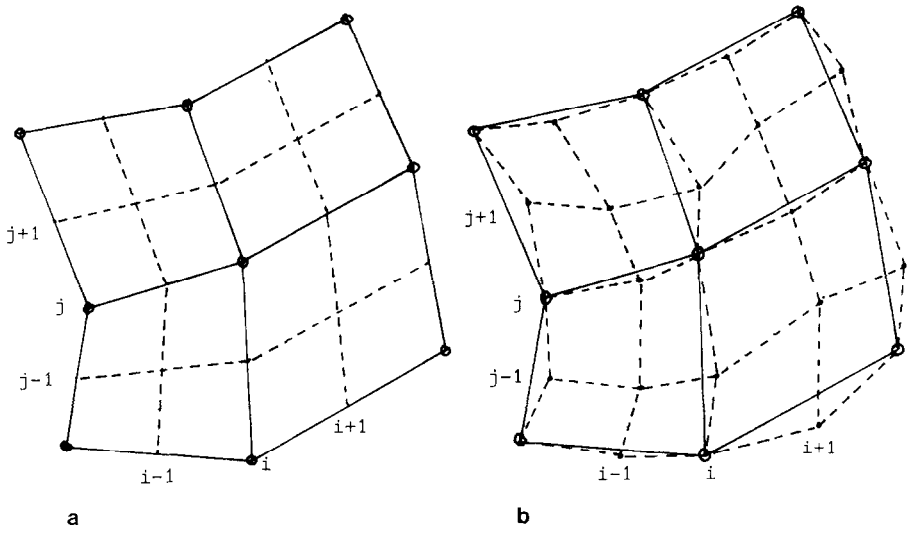

FIG. 2. (a) S_{ij}^{2h} uniformly subdivided mesh. (b) Arbitrarily subdivided mesh.

In the general case with bilinear elements (Fig. 1b), four coefficients are needed for each fine grid meshpoint not coinciding with a coarse grid meshpoint. The computation of these general coefficients (Eq. (21)) is not trivial since $N_{kl}^{2h}(x, y)$ is not explicitly known for an arbitrarily shaped element and one has first to invert the isoparametric transformation (Eq. (9)) to obtain ξ_{ij}^h and η_{ij}^h from

$$x_{ij}^h = \sum_{m,n} x_{m,n}^{2h} N_{m,n}^{2h}(\xi_{ij}^h, \eta_{ij}^h), \tag{23a}$$

$$y_{ij}^h = \sum_{m,n} y_{m,n}^{2h} N_{m,n}^{2h}(\xi_{ij}^h, \eta_{ij}^h), \tag{23b}$$

after which the computation is carried out in the $\xi - \eta$ plane where the basis functions are simple polynomial expressions

$$I_{kl}^{ij} = N_{kl}^{2h}(x_{ij}^h, y_{ij}^h) = N_{kl}^{2h}(\xi_{ij}^h, \eta_{ij}^h). \tag{24}$$

With the bilinear elements for instance, $N^{2h}(\xi, \eta)$ is of the form

$$N^{2h}(\xi, \eta) = \tfrac{1}{4}(1 \pm \xi)(1 \pm \eta) \tag{25}$$

when the four corner points are situated at $(\xi, \eta) = (\pm 1, \pm 1)$.

Fine to Coarse Grid Function Interpolation (Restriction): Operator I_h^{2h}

The value of ϕ^h in the coarse mesh location calculated with the FE approximation in S^h leads to the identity since the coarse gridpoints belong also to the fine grid.

$$[I_h^{2h}\phi^h]_{ij} = \phi^h(x_{ij}^{2h}, y_{ij}^{2h}) = \sum_{k,l} \phi_{kl}^h N_{kl}^h(x_{ij}^{2h}, y_{ij}^{2h}), \tag{26}$$

which due to Eq. (6) reduces to

$$[I_h^{2h}\phi^h]_{ij} = \phi_{ij}^h. \tag{27}$$

This type of restriction is sometimes called injection.

Fine to Coarse Grid Integral Interpolation: Operator ${}^R I_h^{2h}$

As distinct from the FD case, the residual is an integral quantity which is scaled differently on different grids. It cannot be represented in the spaces S^h and S^{2h} and the previous interpolation rules are inapplicable. In the Galerkin approach, the volume integrals are always of the form

$$[R^{2h}(\phi^{2h})]_{ij} = \int_S N_{ij}^{2h}\, g(\phi^{2h})\, dS. \tag{28}$$

For instance, the residual in Eq. (7) can be rewritten in this form with

$$g(\phi^{2h}) = \nabla(\rho(\phi^{2h})\, \nabla\phi^{2h}). \tag{29}$$

A consistent representation of R_{ij}^{2h} by means of fine grid quantities is found by approximating the coarse mesh functions in the integrand of Eq. (28) with fine mesh interpolations in the space S^h, namely,

$$[{}^R I_h^{2h} R^h]_{ij} = \int_{S_{ij}^{2h}} I_h^{2h} N_{ij}^{2h}\, g(I_h^{2h}\phi^h)\, dS, \tag{30}$$

where S_{ij}^{2h} is the coarse mesh residual integration domain, i.e., the part of S where $N_{ij}^{2h} \neq 0$ (Fig. 2).

The interpolation of $\phi^h(x, y)$ to the coarse mesh leads again to the identity since the interpolation of meshpoint values is the identity by virtue of Eq. (27):

$$I_h^{2h}\phi^h(x, y) = \sum_{k,l} N_{kl}^h(x, y)\, I_h^{2h}\phi_{kl}^h = \sum_{k,l} N_{kl}^h(x, y)\, \phi_{kl}^h = \phi^h(x, y). \tag{31}$$

In the same way, the coarse mesh basis function $N_{ij}^{2h}(x, y)$ is approximated in the space S^h

$$I_h^{2h} N_{ij}^{2h}(x, y) = \sum_{k,l} N_{kl}^h(x, y)\, I_h^{2h} N_{ij}^{2h}(x_{kl}^h, y_{kl}^h). \tag{32}$$

By Eqs. (27) and (21), this leads to

$$I_h^{2h} N_{ij}^{2h}(x, y) = \sum_{k,l} N_{kl}^h(x, y)\, I_{ij}^{kl}. \tag{33}$$

The final expression for the coarse mesh residual weighting by means of fine grid quantities is obtained from Eq. (30) by inserting expressions (31) and (33):

$$[{}^R I_h^{2h} R^h]_{ij} = \sum_{k,l} I_{ij}^{kl} \int_{S_{ij}^{2h}} N_{kl}^h(x, y)\, g(\phi^h)\, dS. \tag{34}$$

On a uniformly subdivided coarse mesh (Fig. 2a), it is clear that this general expression reduces to

$$[{}^R I_h^{2h} R^h]^{ij} = \sum_{k,l} I_{ij}^{kl} R_{kl}^h, \tag{35}$$

where the summation extends only over the 9 inner points in the domain S_{ij}^{2h}, since the coefficients I_{ij}^{kl} are zero on and outside the boundaries of S_{ij}^{2h}.

Comparing Eqs. (20) and (35), one concludes that the coarse to fine mesh interpolation I_{2h}^h is the adjoint of the residual weighting ${}^R I_h^{2h}$, since they have transposed coefficient matrices:

$$[I_{2h}^h \phi^{2h}]_{ij} = \sum_{k,l} I_{kl}^{ij} \phi_{kl}^{2h}, \qquad [{}^R I_h^{2h} R^h]_{ij} = \sum_{k,l} I_{ij}^{kl} R_{kl}^h. \tag{36}$$

The following result is obtained for uniform subdivisions (Fig. 2a), which corresponds to the uniform interpolation of Eq. (22):

$$\begin{aligned}[{}^R I_h^{2h} R^h]_{ij} = {} & R_{ij}^h + \tfrac{1}{2}(R_{i,j+1}^h + R_{i,j-1}^h + R_{i-1,j}^h + R_{i+1,j}^h) \\ & + \tfrac{1}{4}(R_{i+1,j+1}^h + R_{i+1,j-1}^h + R_{i-1,j+1}^h + R_{i-1,j-1}^h).\end{aligned} \tag{37}$$

On an arbitrarily subdivided mesh (Fig. 2b), the situation is different due to nonoverlapping integration domains for the coarse and fine meshes. If one is willing to apply formula (35) with summation over the 9 innermost meshpoints in Fig. 2b and with the correct nonuniform coefficients, two sources of errors are introduced with respect to the exact formula, Eq. (34):

First, the contributions of points $(i \pm 1, j \pm 2)$ and $(i \pm 2, j \pm 1)$ lying inside the coarse residual integration domain are omitted. For mildly distorted grids their contributions are negligible since the coefficients I_{ij}^{kl} are small near and are zero on or outside the limits of S_{ij}^{2h}. Furthermore, the integral in Eq. (34) extends over only two fine mesh elements compared to four for the other points.

Second, the fine mesh integration domain for points $(i \pm 1, j \pm 1)$, $(i, j \pm 1)$, and $(i \pm 1, j)$ are not always completely contained in the coarse

mesh domain S_{ij}^{2h}. Again the errors are small since the surface differences are small and moreover, the integrands in Eq. (34) approach zero near the limits of the fine mesh integration domain.

In conclusion, Eq. (35) remains an extremely valuable approximation for Eq. 34 in the arbitrary mesh case, but, of course, only when used with the arbitrary mesh interpolation coefficient I_{ij}^{kl} already known from the nonuniform interpolation.

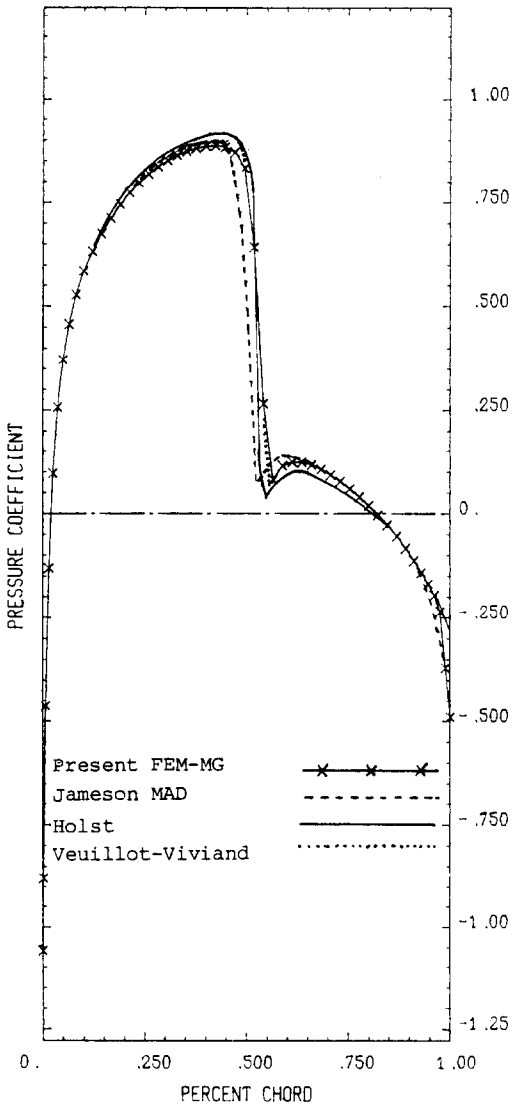

FIG. 3. Comparison with other conservative methods; NACA 0012, $M = 0.80$.

It remains equally valid on the Neumann boundaries of the physical domain, where the summation extends over six fine meshpoints and on the boundary corners, where four meshpoints are used.

The same expression derived here was also obtained for orthogonal meshes by Nicolaides [7] and Brandt [6] based on the minimization approach. Brandt suggests

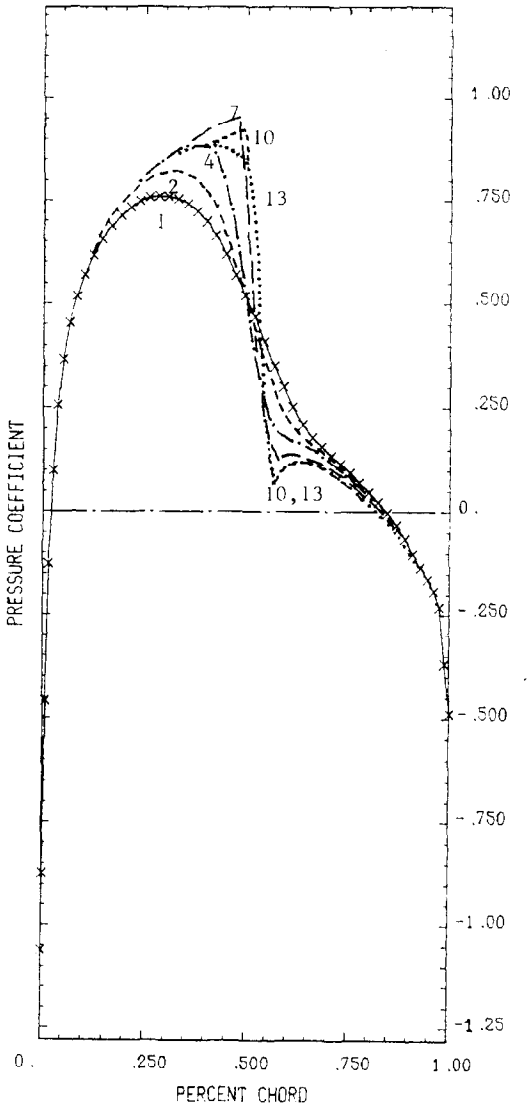

FIG. 4. Evolution of the solution in pseudotime; the number of multigrid cycles is indicated. NACA 0012, $M = 0.80$.

that this *natural* choice is not always better than the residual injection which is given simply by

$$[{}^{R}I_h^{2h}R^h]_{ij} = 4R_{ij}^h \tag{38}$$

in the uniform case.

This has not been confirmed by Nicolaides in his numerical experiments on a square uniform domain. On an arbitrary mesh, residual injection could be constructed with some theoretical support by supposing the function $g(\phi^h)$ constant over the coarse mesh residual integration domain allowing the following approximations:

$$R_{ij}^{2h} \approx g(\phi^{2h}) \int N_{ij}^{2h}\, dS, \qquad R_{ij}^h \approx g(\phi^h) \int N_{ij}^h\, dS, \tag{39}$$

and hence

$$[{}^{R}I_h^{2h}R^h]_{ij} = R_{ij}^h \left(\int N_{ij}^{2h}\, dS \Big/ \int N_{ij}^h\, dS \right), \tag{40}$$

giving exactly expression (38) in the uniform case.

Computational experience with Eq. (40) was highly unsatisfactory and showed that it is inapplicable, at least with the simple smoothing procedure used in this paper.

Computational Results

The convergence of the computation is measured by the evolution of the average residual on the finest grid in terms of the work count which is defined in units representing the work needed for one line relaxation sweep on the finest mesh. For instance, the work count of one complete multigrid cycle with four grids and for the present strategy is given by

$$1 + 2(\tfrac{1}{4} + \tfrac{1}{16}) + \tfrac{10}{64} = 1.91 \text{ units}$$

plus the additional work for the residual weighting and other interpolations. The convergence rate as used below is defined as the mean reduction in the average residual per unit of work. An initial approximate solution on the finest grid for the multigrid iteration is calculated by applying the grid refinement technique with five relaxation sweeps per grid.

All computations are carried out on a fine mesh with 73×25 meshpoints and successively coarser meshes of 37×13, 19×7 and 10×4 meshpoints. Three sets of test cases are presented with different geometric boundary conditions.

The first set is the nonlifting NACA 0012 single airfoil configuration for which the mesh generation method of [17] was adopted. The symmetric lower half part of the mesh was left out, however, since only symmetric nonlifting flows can be treated with the present code which is primarily intended for cascade flow computations.

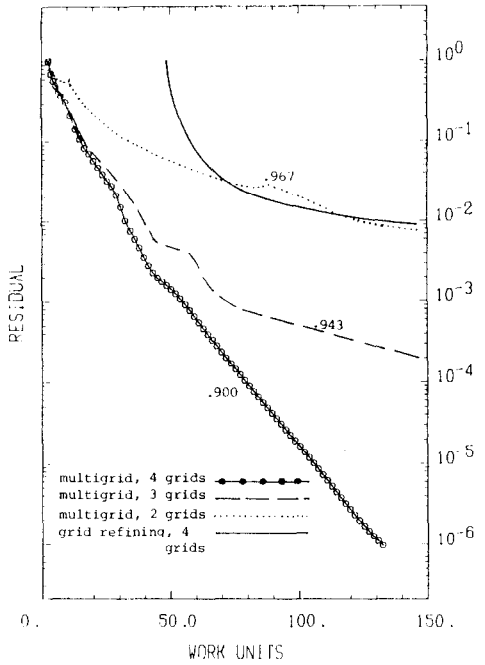

FIG. 5. Convergence history ($M = 0.80$, NACA 0012); convergence rate is indicated.

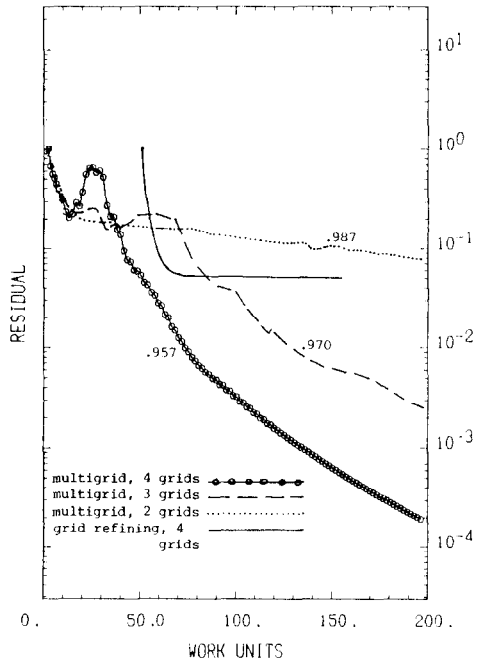

FIG. 6. Convergence history ($M = 0.85$, NACA 0012); convergence rate is indicated.

With a free stream Mach number of 0.80, the standard workshop mesh [17] was used. In Fig. 3, the pressure distribution with a shock of moderate strength is compared with the results obtained by other participants. Good agreement is found. The evolution of the average residual is given in Fig. 5, where the influence of the number of grids is apparent. The convergence rate is improved from 0.967 for 2 grids to 0.900 for 4 grids. The high speed with which the flow pattern is established is illustrated in Fig. 4, where the pressure distribution obtained after 1, 2, 4, 7, 10, and 13 multigrid cycles is shown. The solution is converged after 10 cycles except for a small overshoot ahead of the shock which is suppressed after 13 cycles, when the average residual is still only reduced by 2×10^{-2}.

The residual evolution for the grid refining method is also plotted on Fig. 5, beginning at 50 work units which is the amount of work carried out on the coarse

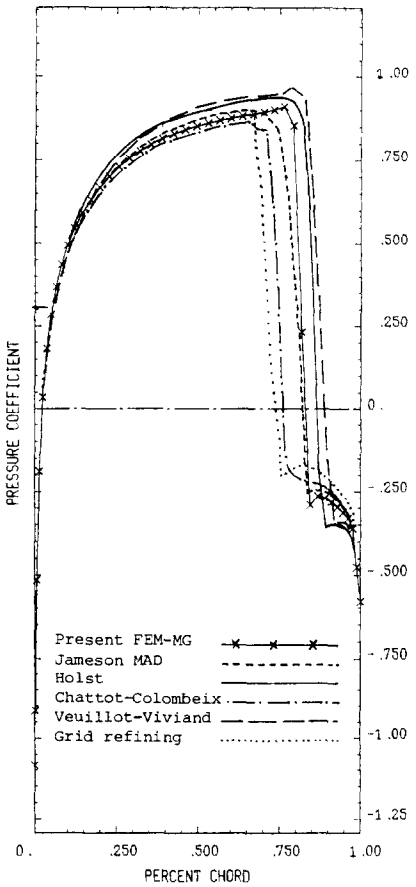

FIG. 7. Comparison with other conservative methods; NACA 0012, $M = 0.85$.

grids before passing to the final mesh. A very fast initial reduction of the mean residual is seen, which corresponds to a fast suppression of the high-frequency errors by the consecutive relaxation sweeps. The remaining low-frequency errors are not eliminated and cause the convergence to slow down after a small number of relaxation steps.

Figure 7 shows the solution for the flow at Mach 0.85 containing a strong shock from $M = 1.4$ to $M = 0.7$. For this solution, the workshop mesh was used with a far field boundary at eight chordlengths from the airfoil. The convergence history is plotted in Fig. 6, showing a rate of 0.957 with four grids. The convergence rate with grid refining approaches 1 after 50 SLOR iterations and in fact, no further improvement of the solution could be obtained although it was not converged as is

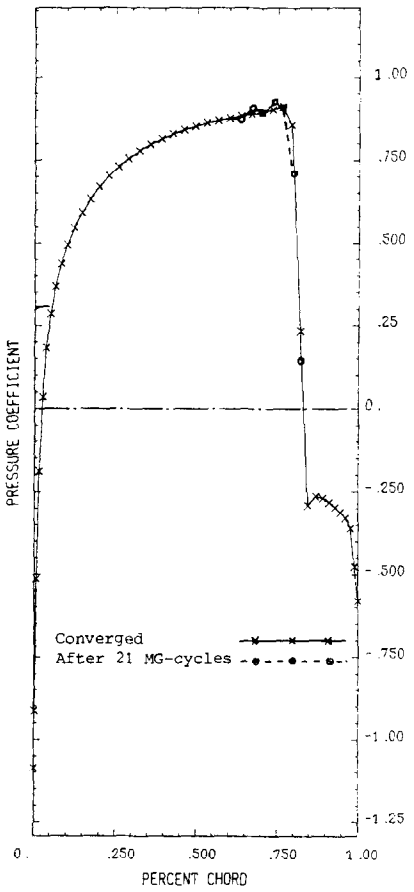

FIG. 8. Comparison of solution after 21 multigrid cycles (50 work units) with converged solution; NACA 0012, $M = 0.85$.

seen by the dotted line in Fig. 7. The nonconverged solution has a sharp shock ahead of the correct converged shock position and is very similar to some of the nonconservative solutions presented in [17]. As can be seen in Fig. 8, the correct shock position with the multigrid scheme is already obtained after 50 work units (21 multigrid cycles) with a mean residual reduction of only 5×10^{-2}, showing again the extremely fast elimination of low-frequency errors.

The second set of results is calculated for a channel flow with a circular bump on the lower wall with the standard workshop mesh [17] which is a sheared Cartesian system. It was given as a test case with an isentropic inlet Mach number of 0.85. This Mach number corresponds to a choked flow for the potential solution, as was confirmed by the results of Veuillot and Viviand while Jameson did not succeed in obtaining a solution for a Mach number higher that 0.835. On the other hand, all

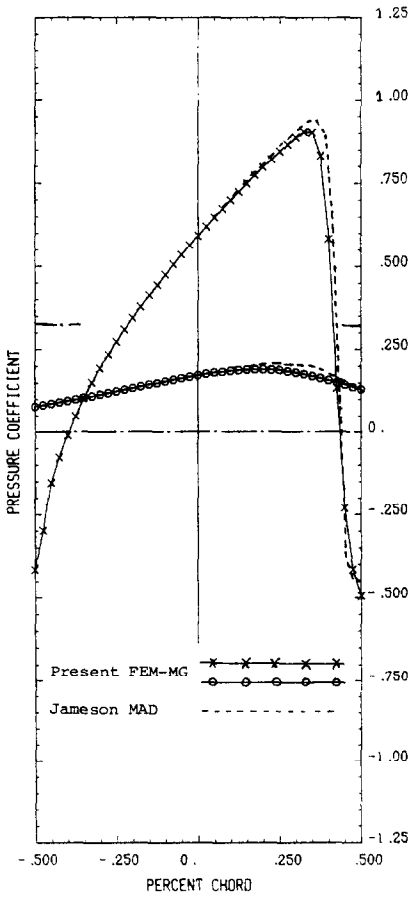

FIG. 9. Channel flow at $M = 0.8435$.

other potential solutions, including our grid refinement solution, were far from choked, namely, with a peak Mach number of ± 0.92 on the upper wall. Again it is clear that this solution is not converged. Indeed, the multigrid solution converges at $M = 0.849$, with a choked solution as is shown in Fig. 10 for the pressure distribution and in Fig. 11 for the isomach lines. In this case, 250 work units were performed with an average residual reduction of 4.2×10^{-2}. The pressure distribution (Fig. 10) is compared with the solution obtained by Veuillot nad Viviand at $M = 0.8500$ with their pseudo-time-dependent fully conservative potential method [17]. Our solution at $M = 0.85$ diverges because the imposed massflow rate at this Mach number is higher than the choking massflow obtained at $M = 0.849$. In Fig. 9, our solution at $M = 0.835$ is compared with the solution of Jameson obtained with his multigrid ADI scheme (MAD) on a 65×17 meshpoint grid allowing 4 or 5 different grids. The

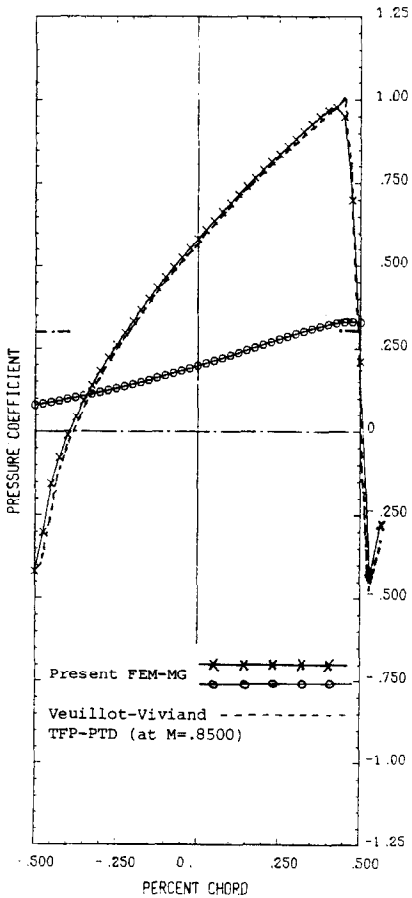

FIG. 10. Channel flow at $M = 0.8490$ (choked).

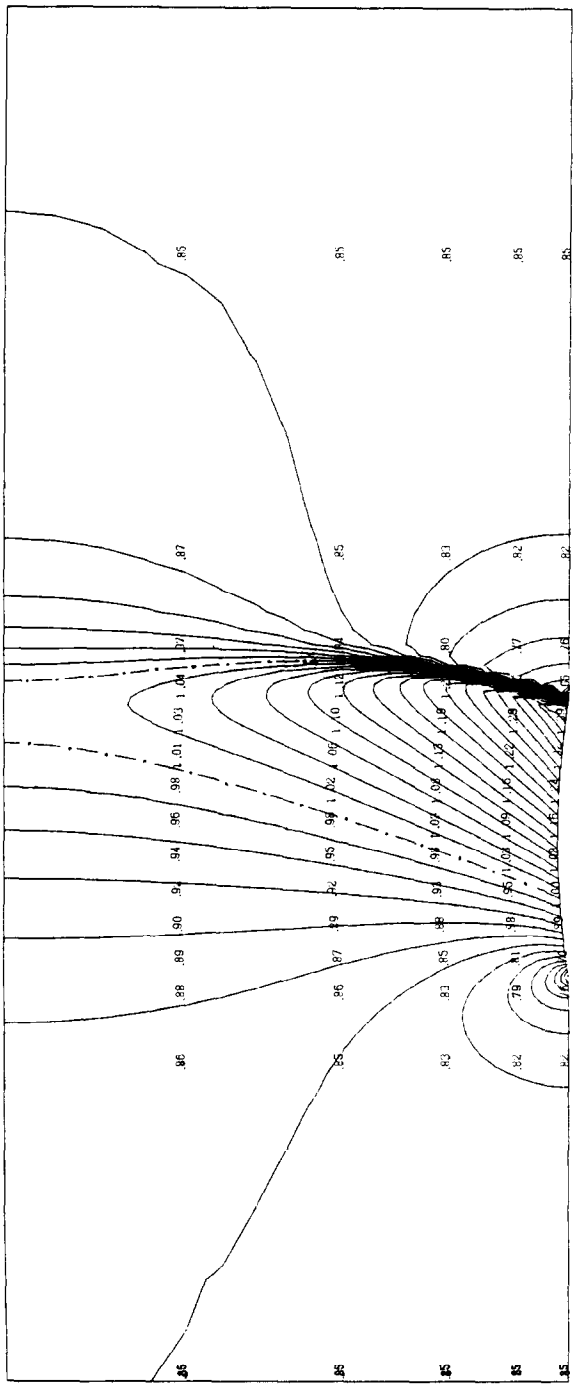

FIG. 11. Choked channel flow at $M = 0.8490$. Isomach lines.

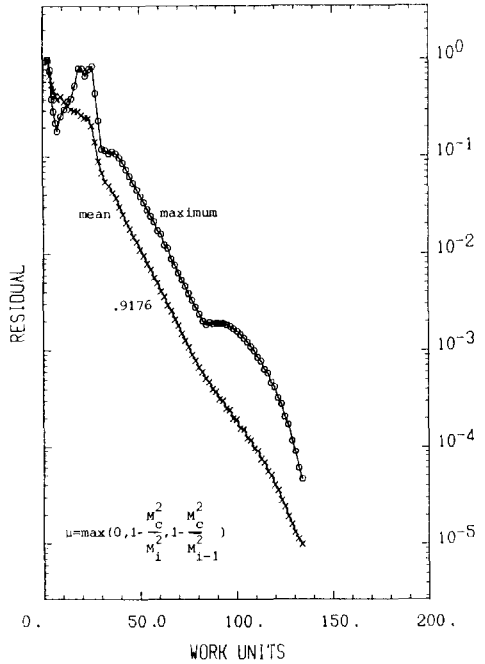

FIG. 12. Channel flow at $M = 0.8435$; convergence history (rate =0.9176).

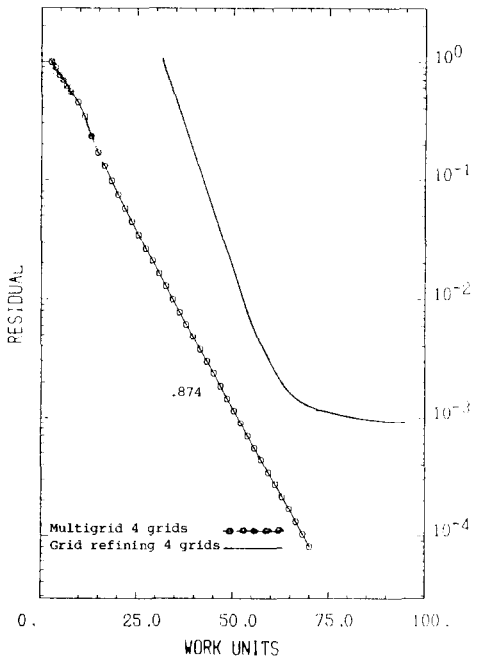

FIG. 13. Subcritical cascade flow. Convergence history (convergence rate is indicated), $M_1 = 0.7000$, $M_2 = 0.4750$, $\beta_1 = 60.20$, $\beta_2 = 50.83$; DCA: $-9.5°$ camber.

residual evolution with our method (Fig. 12) shows a convergence rate of 0.9176. The rate obtained by Jameson with MAD for this case was 0.9742 [17]. For these results, we made use of an improved switching function given by

$$\mu_i = \max(0, 1 - (M_c^2/M_i^2), 1 - (M_c^2/M_{i-1}^2)), \tag{41}$$

where $i-1$ is the upstream element of i.

The final result is a subcritical compressor cascade flow. The mesh is generated by solving a system of elliptic partial differential equations for the curvilinear $\xi - \eta$ coordinates [14]. The convergence history is shown in Fig. 13 and compared with the grid refining. The rate obtained with four grids is 0.874 and illustrates that the periodic and Neumann boundary conditions have no adverse effect on the convergence speed obtained with our multigrid scheme, although no special treatment of the boundaries as suggested by Brandt has been introduced.

Conclusion

A conceptually simple multigrid scheme has been developed consistent with the finite element method and applicable to general arbitrarily generated body fitted grids. Therefore, nonuniform interpolation and residual weighting operators had to be introduced. A fast and reliable method is obtained with the simple straightforward line relaxation scheme as the smoothing step, allowing the calculation of realistic transonic flows with about 10 to 20 multigrid cycles (30 to 50 work units).

References

1. R. P. Fedorenko, *Zh. Vycisl. Mat. Fiz.* **1** (1961), 922.
2. N. S. Bakhvalov, *Zh. Vycisl. Mat. Fiz.* **6** (1966), 861.
3. R. A. Nicolaides, *Math. Comput.* **31** (1977), 892.
4. R. A. Nicolaides, *Math. Comput.* **32** (1978), 1082.
5. W. Hackbusch, "On the Convergence of a Multi-grid Iteration applied to Finite Element Equations," Report 77–8, Math. Inst. Univ. Koln, 1977.
6. A. Brandt, "Multi-level Adaptive Finite Element Methods: I Variational Problems," ICASE Res. Report 79–8, 1979.
7. R. A. Nicolaides, *Math. Compute* **33** (1979), 933.
8. J. C. South and A. Brandt, *in* "Transonic Flow Problems in Turbomachinery" (Adamson and Platzer, Eds.), Hemisphere, Washington, 1977.
9. A. Jameson, "Acceleration of Transonic Potential Flow Calculations on Arbitrary Meshes by the Multiple Grid Method," AIAA Paper 79–1458, 1979.
10. H. Deconinck and C. Hirsch, *in* "Proc. III GAMM Conf. on Num. Meth. in Fluid Mech.," Köln, 1979; Notes on Numerical Fluid Mechanics, Vol. 2, Vieweg, Brunswick, 1980.
11. P. D. Lax, *Commun. Pure Appl. Math.* **7** (1954), 159.
12. M. Hafez, E. M. Murman, and J. C. South, "Artificial Compressibility Methods for Numerical Solution of Transonic Full Potential Equation," AIAA Paper 78–1148, 1978.

13. H. DECONINCK AND C. HIRSCH, *in* "Proc., IV Int. Symp. on Computing Methods in Applied Sciences and Engineering," IRIA, Paris, December 1979.
14. H. DECONINCK AND C. HIRSCH, "Finite Element Methods for Transonic Blade-to-Blade Calculation in Turbomachines," ASME paper 81-GT-5, 1981, presented at the Int. Gas Turbine Conf. and Product Show, Houston, Texas, March 1981.
15. H. DECONINCK AND C. HIRSCH, *in* "Proc. of 7th Int. Conf. Num. Meth. Fl. Dyn.," Stanford, Calif., June 1980.
16. A. BRANDT, *Math. Comput.* **31** (1977), 333.
17. "Numerical Methods for the Computation of Inviscid Transonic Flows with Shock Waves: A GAMM Workshop" (A. Rizzi and H. Viviand, Eds.), Vieweg, Brunswick, 1981.